



Special Feature: Nanostructured Materials

Research Report

Au Nanoparticle-embedded Core/shell Mesoporous Silica Spheres

Hitoshi Kumagai, Tadashi Nakamura and Kazuhisa Yano

Report received on Aug. 6, 2011

■ **ABSTRACT** ■ A series of organically functionalized core/shell monodispersed mesoporous silica spheres (MMSSs) were synthesized and characterized as host materials for Au nanoparticles. The core/shell MMSSs contain bulky propyl groups in the shell and thiol groups as coordination sites for Au ions in the core. The amount and molar ratio of propyl groups in the shell could be systematically controlled by changing the amount and composition of the silica precursor. Au nanoparticles are formed within the core/shell MMSSs and retained within the core after heat treatment due to the steric hindrance and hydrophobic character of the propyl groups in the shell, which act as an effective barrier to migration of the Au nanoparticles. The absorption band of the Au nanoparticles showed a blue-shift with decreasing thickness of the shell and with increasing reduction temperature.

■ **KEYWORDS** ■ Au, Nanoparticle, Core/shell, Silica, Mesoporous, Plasmon

1. Introduction

Noble metal and semiconductor nanoparticles in the nanometer size range display many interesting optical, electronic, and chemical properties depending on their sizes. Such nano-scale materials have potential applications in developing sensors, optoelectronic devices, and catalysts. Among them, Au nanoparticles have attracted significant attention due to their many interesting properties and potential technological applications.⁽¹⁻³⁾ For instance, Au nanoparticles have been used in the field of electrochemistry for applications such as electroanalysis and bioelectroanalysis, particularly in DNA sensing, as well as in electrocatalysis.^(4,5) While bulk Au nanoparticles show negligible catalytic activity, those supported on thin metal oxides show high catalytic activity for a variety of reactions, from combustion to hydrogenation and reduction.^(2,6,7) Au nanoparticles exhibit a strong absorption band in the visible region, which is a small particle effect as evidenced by the lack of an absorption band for individual atoms or for the bulk metal.⁽⁸⁾ In fact, the absorption band originates from the collective oscillation of free conduction electrons in the nanoparticles induced by interaction with the electromagnetic field.⁽⁹⁾ This so-called surface plasmon resonance (SPR) can lead to enhancement of the local electromagnetic field in the vicinity of the Au nanoparticles as observed in surface-enhanced Raman

scattering (SERS) and related techniques, which have been extensively studied.⁽⁸⁾

Mesoporous silica has received considerable attention because of its uniform pore characteristics, high specific surface area, and the controllable pore structures. Many studies have been conducted on the synthesis of mesoporous silicas for applications such as catalysts, adsorbents, and separation columns.⁽¹⁰⁾ In addition, control of the particle shape can provide a variety of morphologies including fibers, sponge-like membranes, rod-like powders, films, and spheres. Controlling the morphology of mesoporous silicas is particularly important for industrial applications. Among the various morphologies, spherical particles are desirable for applications in chromatography, catalysis, drug release and photonics. Spherical mesoporous silica has been synthesized under both acidic and basic conditions. Spherical particles are obtained as a result of minimizing the surface energy, thus the reaction conditions are critical in determining the overall morphology. We have reported on the synthesis of highly monodispersed mesoporous silica spheres (denoted as MMSSs hereafter) that contain ordered starburst (radially aligned) mesopores with hexagonal regularity from tetramethoxysilane (TMOS) and *n*-alkyltrimethylammonium halide.⁽¹¹⁻¹³⁾ Because these MMSSs have radially aligned and highly ordered mesopores, they are highly accessible to guest molecules, enabling the formation of a variety

of nanocomposite spheres incorporating functional materials such as organic dyes, metal oxides, and conducting polymers. Recently, we have focused on the fabrication of functional MMSSs and have reported on magnetic,^(14,15) optical⁽¹⁶⁻¹⁸⁾ and catalytic applications.⁽¹⁹⁻²³⁾ We have made a first step toward the practical use of MMSSs as magnetic or optical materials by incorporating inorganic particles or organic functional molecules in the mesopores. We have also reported core/shell MMSSs in which the catalytic activity is dependent on both the pore size of the MMSSs and the thickness of the shell.⁽²²⁾

Herein we describe our recent work on the fabrication of thiol-functionalized MMSSs via surfactant-directed co-condensation of TMOS and 3-mercaptopropyltrimethoxysilane (MPTMS), and subsequent encapsulation of Au nanoparticles within the MMSSs. The thiol group was selected to encapsulate Au nanoparticles within the mesopores of MMSS because thiol-functionalized organic molecules are often used for the synthesis of encapsulated Au or metal sulfide nanoparticles as well as for the selective adsorption of heavy metal ions. We also describe the optical properties of the Au nanoparticle-embedded MMSSs. In our previous study, the MMSSs having thiol groups retained most of the gold particles within the silica spheres, while some of the Au particles migrated to the outer surface.⁽²⁴⁾ For many applications such as catalysis, optical sensing, and drug delivery, it is desirable to include all of the Au nanoparticles within the mesopores of the silica spheres. To fix the Au nanoparticles within the mesopores of the MMSSs, we further developed thiol-functionalized MMSSs in a series of core/shell MMSSs with thiol groups at the core and propyl groups in the shell. The thiol groups play an important role in the adsorption of AuCl_4^- ions within the core and the propyl groups act as a barrier to migration of the Au particles from inside the core due to their steric hindrance and hydrophobic character.

2. Experimental Section

Tetramethoxysilane (TMOS, Tokyo Kasei), 3-mercaptopropyltrimethoxysilane (MPTMS, Aldrich), propyltrimethoxysilane (PrTMS, Aldrich), hydrogen tetrachloroaurate (Aldrich), *n*-hexadecyltrimethylammonium chloride (C_{16} -TMACl, Tokyo Kasei), 1 M sodium hydroxide solution (Wako Inc.), methanol (Wako Inc.), ethanol (Wako Inc.),

Fluorol 555 (Exciton), and concentrated hydrochloric acid (Wako Inc.) were used without further purification.

2.1 Synthesis of Thiol-functionalized MMSSs without Shell

Thiol-functionalized MMSSs without shell were synthesized employing a previously reported procedure using C_{16} -TMACl as a surfactant.⁽²⁴⁾ The molar ratio of the reagents was 1 TMOS + MPTMS : x MPTMS : 1.27 C_{16} -TMACl : 0.26 NaOH : 1439 methanol : 2560 H_2O , where x was varied from 0 to 1.0. For example, in the case of $x = 0.2$, C_{16} -TMACl (3.52g) and 1 M sodium hydroxide solution (2.28 ml) were combined in 800g of a methanol–water (50 : 50 w/w) mixture. TMOS (1.06g) and MPTMS (0.34g) were mixed under a nitrogen atmosphere and added to the solution under vigorous stirring at 298 K. Several minutes after the addition of the silica source, the clear solution turned opaque. The mixture was then stirred for 8 h and aged overnight without stirring at room temperature. The resulting white precipitate was filtered off and washed with distilled water, before drying at 45°C for 72 h. To extract the surfactant, the dried material (0.7g) was added to a mixture of ethanol (70 mL) and concentrated hydrochloric acid (0.7 mL) at 60°C for 3 h. The surfactant-removed samples were filtered and washed with ethanol, and dried in air. The resultant products are abbreviated as SH($x\%$), where x indicates the ratio of MPTMS in the silica source as described above.

2.2 Synthesis of Core/shell MMSSs

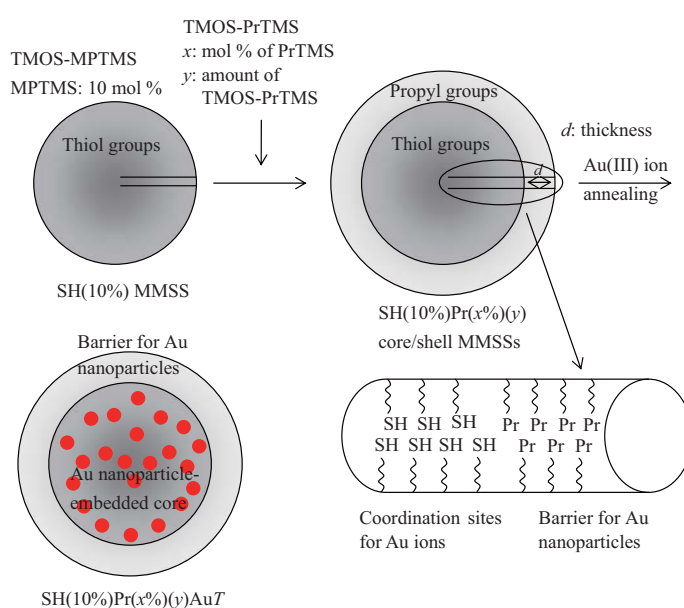
Core/shell MMSSs were prepared using a modification of a procedure reported previously.⁽¹⁰⁾ The core particles of the core/shell MMSSs were first synthesized under the synthetic conditions of SH(10%) as described above. A solution of the SH(10%) core particles was stirred for 1 h before addition of 1 M sodium hydroxide (1.14 ml). To the suspension was then added a TMOS-PrTMS mixture (0.66g). After 8 h of continuous stirring the mixture was aged overnight without stirring. The resulting white precipitate was filtered, washed three times with distilled water, and dried at 70°C for 72 h. Surfactant ions in the mesopores were removed by the same procedure as described above for the thiol-functionalized MMSSs. To prepare a series of

core/shell MMSSs, the amount of TMOS (1.19g)-MPTMS (0.17g) mixture in the core synthesis was fixed, while the amount and PrTMS ratio (mol%) of the TMOS-PrTMS mixture was varied for the shell synthesis (**Scheme 1**). The obtained core/shell MMSSs are designated as SH(10%)Pr($x\%$)(y), where SH(10%) indicates the amount of MPTMS in mol% in the TMOS-MPTMS mixture in the core synthesis, x shows the molar ratio in mol% of PrTMS in the TMOS-PrTMS mixture and y shows the amount of TMOS-PrTMS in grams in the shell ($y = 1, 1/2$ and $1/4$ represent 1.32, 0.66 and 0.33g of TMOS-PrTMS, respectively).

Au nanoparticle-embedded core/shell MMSSs were prepared using the procedure described below.⁽²⁴⁾ The SH(10%)Pr($x\%$)(y) MMSSs (0.5g) were added to an aqueous HAuCl₄ solution (0.3g HAuCl₄ added as 30 wt% solution in dilute hydrochloric acid, Aldrich) and stirred at room temperature for 10 min. The mixture was filtered and washed repeatedly with copious amounts of hydrochloric acid solution (pH 2) to remove any AuCl₄⁻ ions adsorbed on the outer surface of the MMSSs until the filtrate turned colorless and clear. The treated SH(10%)Pr($x\%$)(y)Au was annealed at different temperatures under a flow of 5% H₂-N₂ for 6 h to form Au nanoparticle-embedded spheres. Hereinafter, the obtained samples are abbreviated as SH(10%)Pr($x\%$)(y)Au T , where T indicates the annealing temperature.

2.3 Characterization

A scanning electron microscope (SEM) equipped with an energy-dispersive X-ray (EDX) detector (Hitachi High-Technologies Corporation, S-3600N) at an acceleration voltage of 15 kV was used to determine particle morphology and the elemental composition. Over 50 particles in each SEM image were used to calculate the average particle size of the MMSSs. It should be noted that only a sample of the SEM images is shown in the Figures and particles not appearing in the Figures were also examined. Transmission electron microscope (TEM) images were observed with a JEOL-200CX TEM using an acceleration voltage of 200 kV. Nitrogen adsorption isotherms were measured using a Belsorp-mini II (BEL Japan) at 77 K. Each sample was treated under a pressure of 10⁻³ Torr at 373 K before the nitrogen adsorption measurements. The pore diameter was calculated using the Barrett–Joyner–Halenda (BJH) method. The specific surface area was calculated using the Brunauer–Emmett–Teller (BET) plot for the adsorption branch. X-ray diffraction measurements were carried out with a Rigaku Rint-TTR X-ray diffractometer using Cu radiation. The absorption spectra were measured using a JASCO V-560 spectrophotometer. Thermogravimetric (TG) analyses were performed on a Shimadzu TGA-50 TG-DTA system.



Scheme 1 Schematic of the synthesis of core/shell MMSSs having thiol groups in the core and propyl groups in the shell.

3. Results and Discussion

3.1 Synthesis of Monodispersed Thiol-functionalized MMSSs

In this work, thiol-functionalized MMSSs were designed as host materials for Au nanoparticles. The thiol-functionalized MMSSs were synthesized via co-condensation of TOS and MPTMS. In previous co-condensation syntheses of organo-functionalized mesoporous silicas, it has been found that the resulting morphology depends on the type and concentration of the organoalkoxysilane used. However, in our reaction system no morphological changes were apparent upon incorporation of the organic moiety. While the MMSSs are obtained from reaction between TMOS and a surfactant under very specific conditions, thiol-functionalized MMSSs were prepared over a wide range of x values and spherical particles were obtained in all compositions. SEM observation and EDX analysis revealed that the spherical particles obtained were uniform in size and that their sulfur contents were nearly equal to that in the silica source over the whole range of x values. These results indicate that the spheres were produced as a result of the co-condensation of TMOS and MPTMS.

3.2 Synthesis of Core/shell MMSSs

From the results of in situ TEM observation and XRD measurements, we proposed a particle growth mechanism for the MMSSs.⁽¹⁰⁾ In this mechanism, small particles emerge immediately after the start of synthesis, and then the residual silica precursor reacts preferentially with the surface silanols on these existing particles. This formation mechanism allows for the synthesis of highly monodispersed core/shell mesoporous silica spheres having different chemical properties. This formation mechanism suggests that by changing the silica precursor we have the ability to control not only the thickness of the shell but also its chemical properties, such as the hydrophobic or hydrophilic character, steric hindrance and coordination ability to metal ions. In the present case, thiol and propyl groups are introduced to the core/shell MMSSs to act as a coordination site in the core and a barrier in the shell. That is, sulfur containing ligands are widely used in the synthesis of Au nanoparticles, and the propyl group was introduced as a barrier to prevent migration of the Au nanoparticles. The size of

the propyl group is suitable for entry of the Au precursor and also provides sufficient steric hindrance to prevent migration of the Au nanoparticles formed in the core. We synthesized core/shell MMSSs containing thiol groups in the core and propyl groups in the shell by addition of a TMOS and PrTMS mixture after formation of particles from the initial precursor mixture of TMOS and 10 mol% MPTMS. This reaction yields core/shell MMSSs containing thiol groups as coordination sites in the core and sterically hindered propyl groups in the shell (Scheme 1). The amounts and ratios of the TMOS-PrTMS mixture were changed to optimize the number of propyl groups and the thickness of the shell. Subsequent SEM measurements gave information on the size and morphology of the particles obtained from the reaction. From the SEM images, it was found that all the samples had retained their monodispersed characteristics. The diameters of the particles were dependent on the amount of TMOS-PrTMS mixture added, as summarized in **Table 1**.

The steric hindrance of propyl groups in the shell was controlled by changing the PrTMS/TMOS ratio. Results of nitrogen adsorption-desorption isotherms for the core/shell MMSSs synthesized under different PrTMS/TMOS ratios are summarized in **Fig. 1** and **Table 1**, respectively. These samples showed type IV isotherms similar to those of other MMSSs with or without organic functional groups.⁽²²⁾ When the co-condensation ratio of PrTMS increased, the pore volume decreased due to steric hindrance of the propyl groups in the shell. Similar behavior was observed in amino-functionalized MMSSs.⁽²¹⁾ In the present work, nitrogen adsorption was observed for SH(10%)Pr(75%)(1) and SH(10%)Pr(100%)(1) MMSSs whereas the pore volume abruptly decreased. Thus the SH(10%)Pr(75%)(1) and SH(10%)Pr(100%)(1) MMSSs exhibited the largest pore size and the smallest specific surface area. It is considered that steric hindrance from the propyl groups in the shell prevents adsorption of nitrogen within the core. Although the SH(10%)Pr(75%)(1) and SH(10%)Pr(100%)(1) MMSSs showed almost no nitrogen adsorption, the SH(10%)Pr(75%)(1/2) and SH(10%)Pr(75%)(1/4) MMSSs, having a thinner shell, did adsorb a certain amount of nitrogen. These nitrogen adsorption measurements suggest that the SH(10%)Pr(75%)(1/2) and SH(10%)Pr(75%)(1/4) MMSSs have sufficient space to incorporate Au(III) ions into the pores of the mesoporous silica host.

Thermogravimetric analysis (TG) of the SH(10%)

Table 1 Properties of a series of SH(20%) and SH(10%) Pr(x%)(y) MMSSs.

Sample	Shell/core ratio*	Average particle size (nm)	Standard deviation (%)	Pore size (nm)	Specific surface area (m ² /g)	Pore volume (ml/g)
SH(20%)	0	640	3.2	1.7	873	0.44
SH(10%)Pr(0%)(1)	1	634	2.9	2.2	1302	0.74
SH(10%)Pr(10%)(1)	1	471	5.6	1.8	1426	0.65
SH(10%)Pr(25%)(1)	1	695	2.7	1.7	1377	0.58
SH(10%)Pr(50%)(1)	1	628	2.3	1.8	1273	0.40
SH(10%)Pr(75%)(1)	1	652	2.1	2.4	44	0.03
SH(10%)Pr(100%)(1)	1	620	4.1	2.5	5	0
SH(10%)Pr(50%)(3/4)	0.75	588	2.4	1.9	1105	0.54
SH(10%)Pr(50%)(1/2)	0.5	552	2.4	1.9	1203	0.65
SH(10%)Pr(50%)(1/4)	0.25	517	2.8	2.1	1269	0.66
SH(10%)Pr(75%)(1/2)	0.5	557	2.1	2.1	877	0.46
SH(10%)Pr(75%)(1/4)	0.25	503	2.5	1.7	1127	0.49
SH(10%)Pr(100%)(1/4)	0.25	467	1.9	1.9	887	0.42

* molar ratio of silica precursors used for shell and core portions.

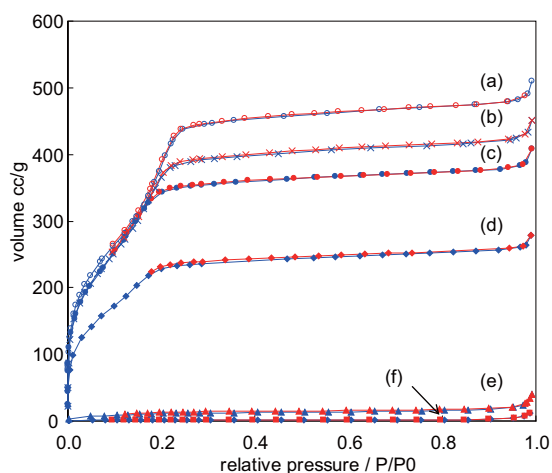


Fig. 1 Nitrogen adsorption-desorption isotherms of (a) SH(10%)Pr(0%)(1), (b) SH(10%)Pr(10%)(1), (c) SH(10%)Pr(25%)(1), (d) SH(10%)Pr(50%)(1), (e) SH(10%)Pr(75%)(1) and (f) SH(10%) Pr(100%)(1) MMSSs.

Pr(10%)(1) MMSSs was performed in an atmosphere of H₂(5%) / N₂ or O₂(20%) / N₂ to investigate the stability of the organic functional groups and the reduction temperature of the Au ions in the MMSSs (**Fig. 2**). The MMSSs show similar behavior up to 240°C in both atmospheres. The MMSSs lose 10 wt% of their weight up to 240°C. The weight loss on heating to 240°C is due to loss of water trapped in the MMSS spheres or adsorbed on the surface of the particles. A

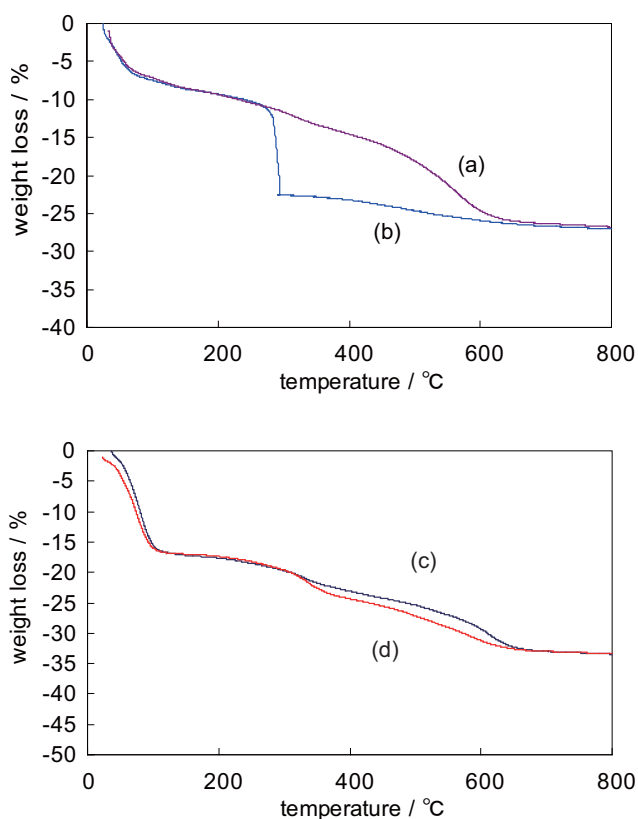


Fig. 2 Thermogravimetric analysis of (a) SHPr(10%)(1) MMSSs under O₂/N₂, (b) SHPr(10%)(1) MMSSs under H₂/N₂, (c) SHPr(10%)(1)Au MMSSs under O₂/N₂, and (d) SHPr(10%)(1)Au MMSSs under H₂/N₂.

change in behavior was observed at around 250°C in the O₂(20%) / N₂ atmosphere, at which point rapid weight loss was observed. This weight loss is attributed to combustion of the organic moieties. On the other hand, in the H₂(5%) / N₂ atmosphere slow weight loss was observed up to 600°C. Here, we assume that the core/shell MMSSs began to lose organic moieties slowly after the initial loss of water molecules but that some organic moieties remained at 250°C. Based on these results we conducted reduction experiments below 250°C.

3.3 Au loading in the Core/shell MMSSs

We synthesized a series of Au-silica composite particles for a core/shell composition of SH(10%)Pr(*x*%)(*y*)Au in a similar procedure to that recently reported.⁽²⁴⁾ The MMSSs were immersed in a HAuCl₄ solution, and upon subsequent filtration, a color change was observed in the MMSSs from white to pale yellow, indicating formation of Au ion-MMSS complexes. The amounts of Au loading were determined by EDX analysis on the SEM to be 9.17, 8.51 and 0.87 wt%, for the SH(10%)Pr(10%)(1)Au, SH(10%)Pr(50%)(1)Au and SH(10%)Pr(75%)(1)Au MMSSs, respectively. The amount of loaded Au ions in the series of core/shell MMSSs decreased as the molar fraction of propyl groups in the shell increased. This result indicates that the propyl groups are acting to prevent Au ions from adsorbing within the core due to steric hindrance, as was suggested by the adsorption–desorption measurements. The amounts of Au ions loaded in the core/shell MMSSs were in the range from 6.13 wt% to 11.78 wt% for the other Au-MMSS composite particles. In addition, when unfunctionalized MMSSs were reacted with HAuCl₄ solution, no Au ions were detected after filtration.⁽²⁴⁾ This indicates that the thiol group acts to adsorb Au ions in the mesopores.

Powder X-ray diffraction (XRD) patterns of the gold-precursor-loaded samples for the SH(10%)Pr(0%)(1)Au, SH(10%)Pr(10%)(1)Au and SH(10%)Pr(50%)(1)Au MMSSs are shown in **Fig. 3**. Sharp peaks are observed between 30° and 80° for the SH(10%)Pr(0%)(1)Au and SH(10%)Pr(10%)(1)Au samples. On the other hand, no peaks were found for the SH(10%)Pr(50%)(1)Au sample. The sharp peaks in the XRD patterns indicate the crystalline structure of gold and these reflections are assigned to the (111), (200), (220), and (311) planes of a face-centered cubic (fcc) gold lattice. The XRD patterns show the

generation of crystalline gold without heat treatment. TEM was used to observe the Au nanoparticles for SH(10%)Pr(10%)(1)Au before heat treatment. Au nanoparticles are found on the surface of the MMSSs, which is indicative of migration of Au nanoparticles from within the mesopores to the outer surface of the MMSSs. Water in the gold-precursor-loaded mesoporous silica plays a key roll in the formation of Au nanoparticles in the mesopores.^(25,26) As evidenced by the easy formation of spherical Au nanoparticles in aqueous solution, the presence of water leads to the formation of spherical, or nearly spherical, gold nanoparticles, possibly due to the large interface energy between gold and water.⁽²⁶⁾ It has also been reported that Au nanoparticles are formed at the pore surface by catalytic reduction of precursor species in the presence of water and that the particles grow along the direction of the pore channels.⁽²⁷⁾ Therefore it is assumed that the Au nanoparticles are formed by the reduction of the gold precursor species within the mesopores of the SH(10%)Pr(0%)(1)Au and SH(10%)Pr(10%)(1)Au MMSSs, with subsequent migration of the gold particles to the surface of the MMSSs. On the other hand, when the host MMSSs were synthesized using a higher PrTMS ratio, the hydrophobic character and steric hindrance of the organic groups in the mesopores increased and the amount of water inside mesopores was decreased. Thus the hydrophobic organic groups prevented the formation of Au nanoparticles and the gold precursors were retained within the mesopore in the SH(10%)Pr(50%)(1) MMSSs before heat treatment.

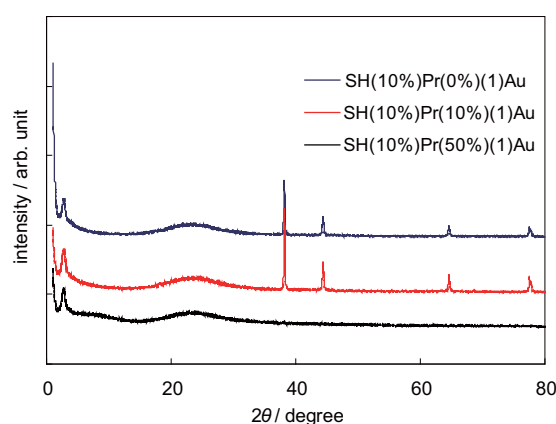


Fig. 3 Powder X-ray diffraction (XRD) patterns of gold-precursor-loaded samples for SH(10%)Pr(0%)(1)Au, SH(10%)Pr(10%)(1)Au and SH(10%)Pr(50%)(1)Au MMSSs.

3.4 Reduction of Gold-precursor-loaded Core/shell MMSSs

The hydrogen reduction at different temperature of MMSSs containing the gold precursor produces Au nanoparticles with different sizes and number densities within the MMSSs. To obtain composite nanostructures for plasmonic and optoelectronic applications it is important to control the size and number densities of Au nanoparticles within the dielectric silica.⁽²⁶⁾ After the reduction, XRD patterns were measured for a series of composite materials in which the amount and PrTMS ratio of the TMOS-PrTMS mixture used in the shell synthesis were changed. First, gold-precursor-loaded core/shell MMSSs synthesized from a 50% TMOS-PrTMS mixture with different amounts of added TMOS-PrTMS were examined, i.e., SH(10%)Pr(50%)(x)Au T ($x = 1, 3/4, 1/2, 1/4; T = 120, 150, 180, 200, 230$). In this series, the amount of TMOS-PrTMS was changed along with the annealing temperature. XRD patterns of the SH(10%)Pr(50%)(1)Au T MMSSs after reduction are shown in **Fig. 4**. Below 100°C, no peaks corresponding to crystalline gold are observed in the XRD pattern. Above 120°C, broad peaks appear in the XRD pattern, at 2θ values between 30° and 80°. These broad peaks correspond to reflections from the (111), (200), (220), and (311) planes of the fcc gold lattice. This result indicates that generation of crystalline gold starts around 120°C. The intensity of these broad peaks increased with

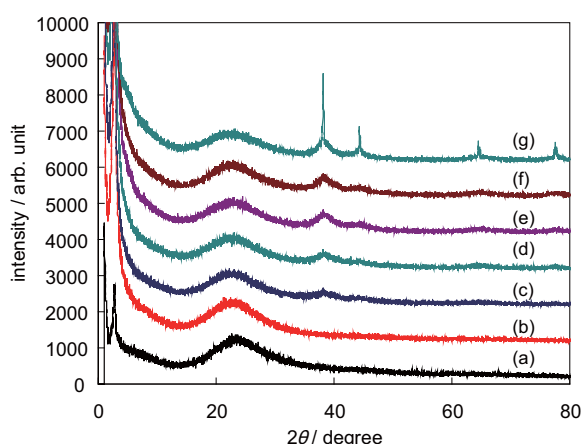


Fig. 4 Powder X-ray diffraction XRD patterns of SH(10%)Pr(50%)(1)Au T MMSSs after heat treatment at different temperatures. (a) before heat treatment, (b) 100°C, (c) 120°C, (d) 150°C, (e) 180°C, (f) 200°C, and (g) 230°C.

increasing reduction temperature. Sharp peaks appear in the XRD pattern of SH(10%)Pr(50%)(1)Au T 30. This result indicates that the Au particles grow and migrate to the outer surface of the MMSSs. The XRD patterns of the SH(10%)Pr(50%)(3/4)Au T MMSSs are similar to those of the SH(10%)Pr(50%)(1)Au T MMSSs. No sharp peaks are apparent in the XRD patterns of the SH(10%)Pr(50%)(3/4)Au T MMSSs up to 200°C. These results indicate that the Au nanoparticles are retained within the MMSS mesopores. On the other hand, sharp peaks are apparent in the XRD pattern of the SH(10%)Pr(50%)(1/2)Au T MMSSs. In the synthesis of SH(10%)Pr(50%)(1/2)Au, the use of only half the amount of the TMOS-PrTMS mixture resulted in a thinner shell for the core/shell MMSSs. Thus the sharp peaks are due to the thin shell and may be caused by thermal sintering leading to the formation of crystalline gold on the surface of the MMSSs at lower temperatures. The XRD pattern of the SH(10%)Pr(50%)(1/4)Au MMSSs exhibits sharp peaks similar to those of the SH(10%)Pr(0%)(1)Au and SH(10%)Pr(10%)(1)Au MMSSs. In this series, it was found that for core/shell MMSSs with a thinner shell, gold nanoparticles were formed at lower temperatures, or even without heat treatment. Next we examined a series of core/shell MMSSs in which the molar ratio of PrTMS in the shell was changed along with the amount of TMOS-PrTMS mixture added, i.e., SH(10%)Pr(75%)(1/2)Au, SH(10%)Pr(75%)(1/4)Au and SH(10%)Pr(100%)(1/4)Au. The SH(10%)Pr(75%)(1/2)Au T MMSSs show similar XRD patterns to those of the SH(10%)Pr(50%)(3/4)Au T and SH(10%)Pr(50%)(1)Au T MMSSs up to 200°C. Sharp peaks are observed in the SH(10%)Pr(75%)(1/4)Au T MMSSs from lower temperatures. From these observations, we conclude that more than half the composition should be silica species and more than 50 mol% of PrTMS should be included in the shell against the core to retain the Au nanoparticles in the MMSS mesopores after heat treatment.

TEM images of the SH(10%)Pr(50%)(1)Au T MMSSs ($T = 120, 150, \text{ and } 180^\circ\text{C}$) are shown in **Fig. 5**. The Au particles (dark areas) are concentrated in the thiol-functionalized core region. The Au particles still remain in the core region after heat treatment and an oval-type structure can be seen. From this oval-type structure observed in the TEM image, the thickness of the shells are found to be 56, 44, and 23 nm for the SH(10%)Pr(50%)(1)Au, SH(10%)Pr(50%)(3/4)Au and SH(10%)Pr(50%)(1/2)Au MMSSs, respectively.

These values are in good agreement with the calculated values based on the amounts of the silica precursors used in the core/shell MMSS synthesis. The thickness of the shell was proportional to the amount of silica source added. The size distribution of the Au nanoparticles in the MMSS after heat treatment ranges from a single nanometer to ca. 15 nm, as indicated by the TEM images. Au nanoparticle-embedded MMSSs without shells have been prepared and reported on previously.⁽²⁴⁾ TEM images indicated that most of the Au particles were confined to within the silica spheres with only some of the Au particles on the outer surface.⁽²⁴⁾ In contrast, in the core/shell MMSSs, the Au particles remained in the core region with no particles observed in the shell region or outer surface. TEM images show that a number of Au particles were

larger than the pore size (ca. 2 nm). This observation indicates that even at temperatures below 200°C the Au particles ruptured the silica pore walls in order to grow larger. Similar particle growth has been reported in other studies on the synthesis of Au nanoparticles confined in mesoporous silicas.^(26,28) The wall thickness of the ordered nanoporous silica (ca. 1 nm) is too thin to prevent the Au nanoparticles from growing during the reduction procedure even at relatively low temperatures (i.e. 200°C).^(26,28)

Diffuse reflectance spectra of the Au nanoparticle-embedded MMSSs obtained at different reduction temperatures, i.e., SH(10%)Pr(50%)(1)AuT ($T = 120, 150, 180, 200^\circ\text{C}$), are shown in **Fig. 6**. The dependence of the peak position on the reduction temperature is shown in **Fig. 7** for the series of SH(10%)Pr(50%)

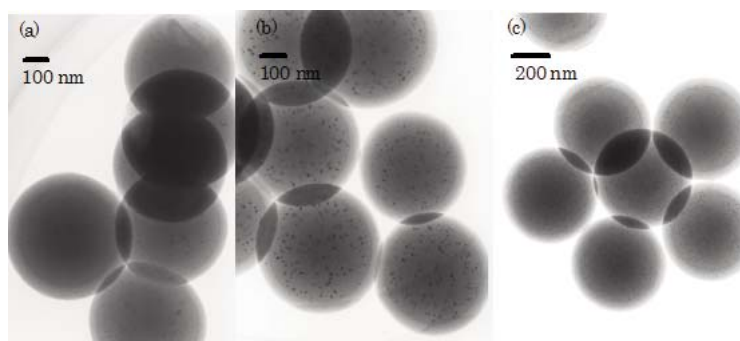


Fig. 5 TEM images of SH(10%)Pr(50%)(1)AuT MMSSs after heat treatment at (a) 120°C, (b) 150°C, and (c) 180°C.

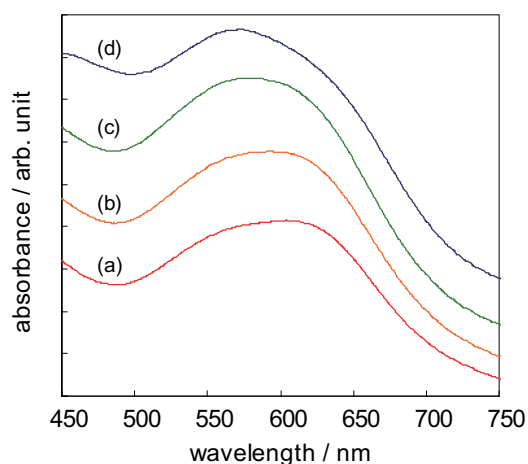


Fig. 6 Diffuse reflectance spectra of SH(10%)Pr(50%)(1)AuT MMSSs after heat treatment at (a) 120°C, (b) 150°C, (c) 180°C, and (d) 200°C.

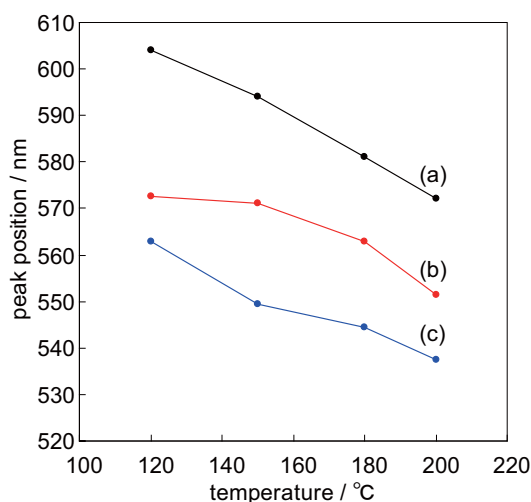


Fig. 7 Plasmon peak positions of SH(10%)Pr(50%)(y)AuT MMSSs for (a) $y = 1$, (b) $y = 3/4$, and (c) $y = 1/2$ samples after heat treatment at different temperatures.

(1)AuT MMSSs. As shown in Fig. 6, the spectrum of the SH(10%)Pr(50%)(1)Au120 MMSSs exhibits a peak with a maximum absorbance at 604 nm and a shoulder at around 550 nm. Figure 7 shows a shift in the absorption maximum from 604 nm to 572 nm with increasing reduction temperature from 120°C to 200°C. The diffuse reflectance spectra of the SH(10%)Pr(75%)(1/2)AuT MMSSs exhibit similar peak shifts to those of the SH(10%)Pr(50%)(1)AuT series. The observed surface-plasmon absorption band of Au depends on several factors including the particle size, shape, surrounding medium and inter-particle interactions, which affect the peak position and intensity.⁽²⁹⁾ Although the size of the Au particles, which range from a single nanometer to ca. 15 nm, is one of the most important factors in determining the peak position of the surface plasmon band, these other factors also strongly affect it.⁽³⁰⁾ It is assumed that if the heat treatment of the gold-precursor-loaded core/shell MMSSs is performed at a lower temperature, then the diameter of the Au nanoparticles will be smaller and the number density of the Au nanoparticles within the core region higher, thus shifting the absorption peak of the resulting composite to a higher wavelength. This behavior is similar to that observed for Au nanoparticle-embedded mesoporous silica nanofibers.⁽²⁶⁾ Also, narrowing of the absorption bands occurs with increasing temperature, indicating that the size distribution range of the Au nanoparticles becomes smaller with increasing temperature. This is considered to be a result of Ostwald ripening, narrowing the range of particle sizes.

Several techniques utilize the interaction between plasmonic materials and dyes and the resulting effect on the optical spectrum of the dyes. To observe their optical properties, we prepared composite materials consisting of Au nanoparticle-embedded MMSSs and an organic dye. The composites were obtained by mixing an organic dye, Fluorol 555 (0.5 mg), with Au nanoparticle-embedded core/shell MMSSs (0.1g) in the solid state, and their emission spectra were measured. **Figure 8** shows preliminary results for the emission spectra of the composites. Although the maximum intensity of the emission spectra seems to depend on the shell thickness of the Au-loaded MMSSs, the effect of another factor such as the plasmon peak wavelength should also be considered.

The Au nanoparticle-embedded samples still have accessible pore channels with high surface area and pore volume as evidenced from nitrogen adsorption

measurements for the SH(10%)Pr(50%)(3/4)Au150 and SH(10%)Pr(75%)(1/2)Au150 MMSSs. However, due to the presence of Au nanoparticles in the mesopores, the surface area and pore volume are smaller than those of the original host materials.

4. Conclusion

A series of organically functionalized core/shell monodispersed mesoporous silica spheres (MMSSs) was synthesized. These core/shell MMSSs contain bulky propyl group, as a barrier in the shell and thiol groups as coordination sites for Au ions in the core.

The amount and molar ratio of the propyl groups in the shell were controlled by adjusting the amount and ratio of the silica precursor. Due to steric hindrance of the propyl groups, Au nanoparticles were retained within the core after heat treatment. The absorption maximum of the Au nanoparticles showed a blue-shift with decreasing thickness of the shell and with increasing reduction temperature. Because the Au nanoparticle-embedded composites obtained herein still have large surface areas and pore volumes, a variety of nanoparticles, functional materials, and proteins, such as quantum dots, dyes, and enzymes can be incorporated. Such composites have potential applications in magneto-optical materials, drug delivery systems, catalysis, and novel plasmonic materials.

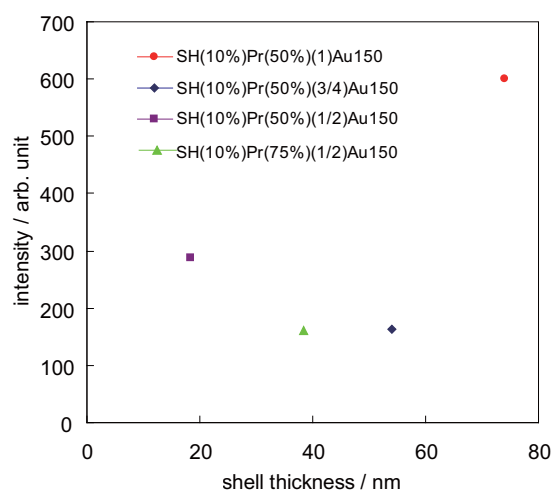


Fig. 8 Effect of shell thickness on emission intensity of Fluorol 555 and core/shell MMSS composites. The peak intensity of the emission at 520 nm is plotted against shell thickness.

References

- (1) Chen, M. and Goodman, D. W., "Catalytically Active Gold: From Nanoparticles to Ultrathin Films", *Acc. Chem. Res.*, Vol.39, No.10 (2006), pp.739-746.
- (2) Daniel, M. C. and Astruc, D., "Gold Nanoparticles: Assembly, Supramolecular Chemistry, Quantum-size-related Properties, and Applications toward Biology, Catalysis, and Nanotechnology", *Chem. Rev.*, Vol.104, No.1 (2004), pp.293-346.
- (3) Jain, P. K., Huang, X., El-Sayed, I. H. and El-Sayed, M. A., "Noble Metals on the Nanoscale: Optical and Photothermal Properties and Some Applications in Imaging, Sensing, Biology, and Medicine", *Acc. Chem. Res.*, Vol.41, No.12 (2008), pp.1578-1586.
- (4) Chang, H. X., Yuan, Y., Shi, N. L. and Guan, Y. F., "Electrochemical DNA Biosensor Based on Conducting Polyaniline Nanotube Array", *Anal. Chem.*, Vol.79, No.13 (2007), pp.5111-5115.
- (5) Dai, X., Wildgoose, G. G., Salter, C., Crossley, A. and Compton, R. G., "Electroanalysis Using Macro-, Micro-, and Nanochemical Architectures on Electrode Surfaces. Bulk Surface Modification of Glassy Carbon Microspheres with Gold Nanoparticles and Their Electrical Wiring Using Carbon Nanotubes", *Anal. Chem.*, Vol.78, No.17 (2006), pp.6102-6108.
- (6) Choudhary, T. V. and Goodman, D. W., "Catalytically Active Gold: The Role of Cluster Morphology", *Appl. Catal. A: General*, Vol.291, No.1-2 (2005), pp.32-36.
- (7) Crooks, R. M., Zhao, M. Q., Sun, L., Chechik, V. and Yeung, L. K., "Dendrimer-encapsulated Metal Nanoparticles: Synthesis, Characterization, and Applications to Catalysis", *Acc. Chem. Res.*, Vol.34, No.3 (2001), pp.181-190.
- (8) Ghosh, S. K. and Pal, T., "Interparticle Coupling Effect on the Surface Plasmon Resonance of Gold Nanoparticles: From Theory to Applications", *Chem. Rev.*, Vol.107, No.11 (2007), pp.4797-4862.
- (9) Link, S. and El-Sayed, M. A., "Spectral Properties and Relaxation Dynamics of Surface Plasmon Electronic Oscillations in Gold and Silver Nanodots and Nanorods", *J. Phys. Chem. B*, Vol.103, No.40 (1999), pp.8410-8426.
- (10) Nakamura, T., Mizutani, M., Nozaki, H., Suzuki, N. and Yano, K., "Formation Mechanism for Monodispersed Mesoporous Silica Spheres and Its Application to the Synthesis of Core/shell Particles", *J. Phys. Chem. C*, Vol.111, No.3 (2007), pp.1093-1100.
- (11) Yano, K. and Fukushima, Y., "Particle Size Control of Mono-dispersed Super-microporous Silica Spheres", *J. Mater. Chem.*, Vol.13, No.10 (2003), pp.2577-2581.
- (12) Yano, K. and Fukushima, Y., "Synthesis of Mono-dispersed Mesoporous Silica Spheres with Highly Ordered Hexagonal Regularity Using Conventional Alkyltrimethylammonium Halide as a Surfactant", *J. Mater. Chem.*, Vol.14, No.10 (2004), pp.1579-1584.
- (13) Yano, K., Suzuki, N., Akimoto, Y. and Fukushima, Y., "Synthesis of Mono-dispersed Mesoporous Silica Spheres with Hexagonal Symmetry", *Bull. Chem. Soc. Jpn.*, Vol.75, No.9 (2002), pp.1977-1982.
- (14) Mizutani, M., Yamada, Y., Nakamura, T. and Yano, K., "Anomalous Pore Expansion of Highly Monodispersed Mesoporous Silica Spheres and Its Application to the Synthesis of Porous Ferromagnetic Composite", *Chem. Mater.*, Vol.20, No.14 (2008), pp.4777-4782.
- (15) Nakamura, T., Yamada, Y. and Yano, K., "Novel Synthesis of Highly Monodispersed Gamma-Fe₂O₃/SiO₂ and Epsilon Fe₂O₃/SiO₂ Nanocomposite Spheres", *J. Mater. Chem.*, Vol.16, No.25 (2006), pp.2417-2419.
- (16) Yamada, H., Nakamura, T., Yamada, Y. and Yano, K., "Colloidal-crystal Laser Using Monodispersed Mesoporous Silica Spheres", *Adv. Mater.*, Vol.21, No.41 (2009), pp.4134-4138.
- (17) Yamada, Y., Nakamura, T., Ishii, M. and Yano, K., "Reversible Control of Light Reflection of a Colloidal Crystal Film Fabricated from Monodisperse Mesoporous Silica Spheres", *Langmuir*, Vol.22, No.6 (2006), pp.2444-2446.
- (18) Yamada, Y., Nakamura, T. and Yano, K., "Optical Response of Mesoporous Synthetic Opals to the Adsorption of Chemical Species", *Langmuir*, Vol.24, No.6 (2008), pp.2779-2784.
- (19) Suzuki, T. M., Mizutani, M., Nakamura, T., Akimoto, Y. and Yano, K., "Pore-expansion of Organically Functionalized Monodispersed Mesoporous Silica Spheres and Pore-size Effects on Adsorption and Catalytic Properties", *Microporous Mesoporous Mater.*, Vol.116, No.1-3 (2008), pp.284-291.
- (20) Suzuki, T. M., Nakamura, T., Akimoto, Y. and Yano, K., "Catalytic Performance of Organically Functionalized Core/shell Monodispersed Mesoporous Silica Spheres Containing an Adsorption Layer", *Chem. Lett.*, Vol.37, No.1 (2008), pp.124-125.
- (21) Suzuki, T. M., Nakamura, T., Fukumoto, K., Yamamoto, M., Akimoto, Y. and Yano, K., "Direct Synthesis of Amino-functionalized Monodispersed Mesoporous Silica Spheres and Their Catalytic Activity for Nitroaldol Condensation", *J. Mol. Catal. A-Chem.*, Vol.280, No.1-2 (2008), pp.224-232.
- (22) Suzuki, T. M., Nakamura, T., Sudo, E., Akimoto, Y. and Yano, K., "Enhancement of Catalytic Performance by Creating Shell Layers on Sulfonic Acid-functionalized Monodispersed Mesoporous Silica Spheres", *J. Catal.*, Vol.258, No.1 (2008), pp.265-272.
- (23) Suzuki, T. M., Nakamura, T., Sudo, E., Akimoto, Y. and Yano, K., "Synthesis and Catalytic Properties of Sulfonic Acid-functionalized Monodispersed Mesoporous Silica Spheres", *Microporous*

Mesoporous Mater., Vol.111, No.1-3 (2008), pp.350-358.

- (24) Nakamura, T., Yamada, Y. and Yano, K., "Direct Synthesis of Monodispersed Thiol-functionalized Nanoporous Silica Spheres and Their Application to a Colloidal Crystal Embedded with Gold Nanoparticles", *J. Mater. Chem.*, Vol.17, No.35 (2007), pp.3726-3732.
- (25) Fukuoka, A., Higuchi, T., Ohtake, T., Oshio, T., Kimura, J., Sakamoto, Y., Shimomura, N., Inagaki, S. and Ichikawa, M., "Nanonecklaces of Platinum and Gold with High Aspect Ratios Synthesized in Mesoporous Organosilica Templates by Wet Hydrogen Reduction", *Chem. Mater.*, Vol.18, No.2 (2006), pp.337-343.
- (26) Tsung, C. K., Hong, W. B., Shi, Q. H., Kou, X. S., Yeung, M. H., Wang, J. F. and Stucky, G. D., "Shape- and Orientation-controlled Gold Nanoparticles Formed within Mesoporous Silica Nanofibers", *Adv. Funct. Mater.*, Vol.16, No.17 (2006), pp.2225-2230.
- (27) Ge, J. P., Zhang, Q., Zhang, T. R. and Yin, Y. D., "Core-satellite Nanocomposite Catalysts Protected by a Porous Silica Shell: Controllable Reactivity, High Stability, and Magnetic Recyclability", *Angew. Chem. Int. Ed.*, Vol.47, No.46 (2008), pp.8924-8928.
- (28) Chi, Y. S., Lin, H. P. and Mou, C. Y., "CO Oxidation over Gold Nanocatalyst Confined in Mesoporous Silica", *Appl. Catal. A: General*, Vol.284, No.1-2 (2005), pp.199-206.
- (29) Makarova, O. V., Ostafin, A. E., Miyoshi, H., Norris, J. R. and Meisel, D., "Adsorption and Encapsulation of Fluorescent Probes in Nanoparticles", *J. Phys. Chem. B*, Vol.103, No.43 (1999), pp.9080-9084.
- (30) Liz-Marzan, L. M., "Tailoring Surface Plasmons through the Morphology and Assembly of Metal Nanoparticles", *Langmuir*, Vol.22, No.1 (2006), pp.32-41.

Figs. 1 and 3-7

Reprinted from *Chem. Mater.*, Vol.22, No.17 (2010), pp.5112-5118, Kumagai, H. and Yano, K., Synthesis and Characterization of Au-loaded Core/shell Mesoporous Silica Spheres Containing Propyl Group in the Shell, © 2010 ACS, with permission from American Chemical Society.

Hitoshi Kumagai

Research Fields:

- Materials Chemistry
- Coordination Chemistry

Academic Degree: Dr. Sci.

Academic Society:

- The Chemical Society of Japan



Tadashi Nakamura

Research Fields:

- Inorganic Materials Chemistry
- Solid State Electrochemistry

Academic Degree: Dr. Eng.

Academic Societies:

- The Chemical Society of Japan
- The Ceramic Society of Japan
- The Electrochemical Society of Japan

Award:

- Award of the Outstanding Papers Published in the JCSJ in 2004



Kazuhisa Yano

Research Fields:

- Porous Materials
- Colloidal Crystals

Academic Degree: Dr. Eng.

Academic Society:

- American Chemical Society

